Modeling and Simulation of Thermodynamic Processes of Vertical Shaft Kiln Used for Producing Deadburned Magnesia

M.G. Rasul and D. Saotayanan

***Abstract*—**A computational fluid dynamics (CFD) modeling and simulation of thermodynamic processes of vertical shaft kiln used for producing deadburned magnesia is presented. The model developed is a 2D steady state model. The combustion, particle-gas dynamics and heat transfer processes which occur inside a vertical shaft kiln are modeled by Eulerian multiphase model, and Species transport and finite volume chemical reaction model. Segregated solver is employed to solve and couple the numerical calculations from each model. Numerical approach and computational methodology are detailed. The simulated results on gas and granular bed temperatures as a function of kiln height are discussed and compared with the designed data. The simulated results show a reasonably good agreement with the designed data supplied by reference plant.

***Keywords*—**Shaft kiln, thermodynamic processes, modeling and simulation, CFD code FLUENT.

I. Introduction

The vertical shaft kiln is a high temperature processing unit in the production of deadburned magnesia [1, 2]. After raw magnesite ($MgCO_3$) is processed through a multiple heart furnace and converted into calcined magnesite (MgO) or clinker, it is further processed through vertical shaft kilns where densification or deadburned process occurs at approximately 2300 ^oC. The bulk density of MgO briquettes are from 1910 kg/m^3 to 3540 kg/m^3 during 7-8 hours of holding time. The quality of the final product is governed by uniformity in heat distribution, fuel types, gas-briquettes contact, fuel to briquettes ratio, permeability, airflow/drought, holding time and insulation efficiency. During the operation, compact MgO briquettes (Clinker) is fed through the top of the kiln and onto the existing packed bed which progresses down the vertical shaft body continuously by the influence of the gravitational force. The packed bed of MgO briquettes react with the counterflow of hot gas resulting from combustion, absorbing energy and momentum which gives them translational and rotational motions and in turn affecting the gas flow.

Manuscript received February 26, 2007: Revised version received May 31, 2007.

M. G. Rasul is a Senior Lecturer at Central Queensland University, Rockhampton, Queensland 4702, Australia (phone: 61 7 4930 9676, fax: 61 7 4930 9382, e-mail: m.rasul@cqu.edu.au).

S. Saotayanan is aGraduate Mechanical Engineer at Lead Smelter, Xstrata Zinc Mt Isa, Australia (email: dsaotayanan@xstratazinc.com.au) .

The combustion in the kiln is fuelled by the combination of natural gas and air which injected through fuel injectors annularly mounted around the middle level of the kiln. The heat generated from combustion process flows through the packed bed and transferred to the briquettes via convection and radiation, raising the temperature of the downward moving bed and causing densification process to take place which turns the clinker into final deadburned product. Prior to discharge, the hot deadburned product is cooled by secondary air and water injected from the bottom of the kiln. Fig.1 shows simplified schematic of processes involved in an annular vertical shaft kiln [1]. It consists of top end entry for the green briquettes, exhaust vent on the top of the kiln, four levels of fuel distributors; only one level is operated at one time, natural gas inlet and primary air inlet, bottom ring cone, flat turn table, bottom discharge cone, secondary air inlet and product discharge sealed pipe.

A number of people tried to develop mathematical models for the thermodynamic process of the shaft kiln using either Lotus-123 or MatLab; while they are useful the models did not provide accurate prediction due to over simplification of the processes involved [3-5]. In this study, a CFD model is developed using CFD code FLUENT with an aim to achieve more accurate prediction of thermodynamic processes inside shaft kiln. This approach takes into an account of the interacting physical and chemical laws of combustion, particle gas dynamics, and mass and heat transfer, all of which are results from interactions between natural gas-air combustion and the continuous moving packed bed of briquettes inside the kiln.

II. Process Description

The process of combustion, heat transfer and particle dynamics which occur in normal operation of vertical shaft kiln at Magnesia plant are described below:

A. Combustion

The primary sources of combustion reaction occur in the shaft kiln include oxygen (exists in the primary and secondary air) and methane (exists in the injected natural gas). Due to excessive supply of oxygen into the shaft kiln, the type of combustion takes place is considered as complete. It is to be noted that methane takes up about 89% of the total combustible components in natural gas, and thus, only the reaction kinetic of methane and oxygen is considered in this study. The effect of thermal decomposition is neglected in the

model, this is due to the fact that the dissociation and ionization reaction are limited to only reaction at a higher temperature than that which takes place in the reference kiln. The schematic diagram of simplified combustion system of the kiln is shown in Fig.2. On the left hand side (reactant) natural gas mixes with oxygen, and undergoes complete combustion which produces carbon dioxide and water vapor as shown on the right hand side (product), while heat is transferred from the system to the surrounding.

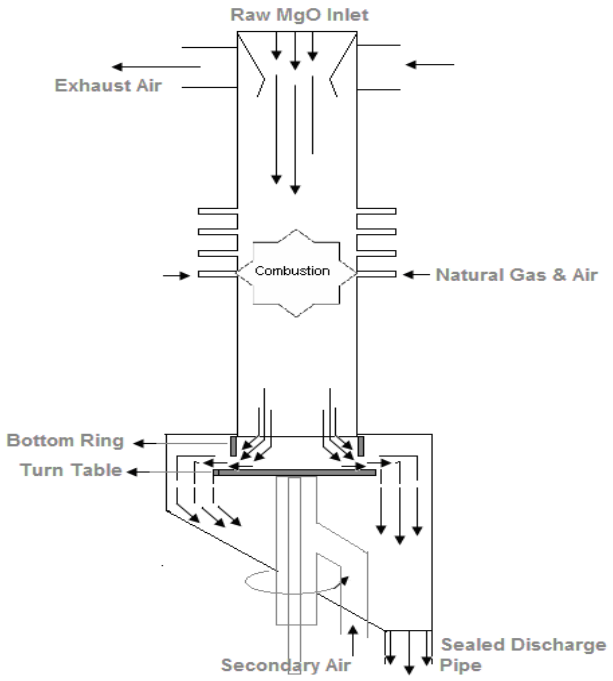

Fig.1 Simplified process of vertical shaft kiln

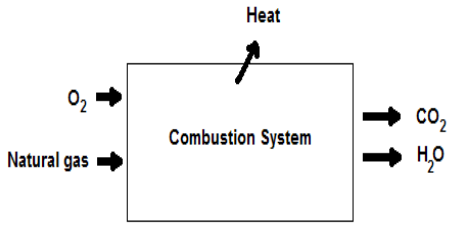

Fig.2 Schematic diagram of the combustion system in the kiln

The amount of heat release from combustion is simply the difference between the enthalpy required to form the compound of the products and that of the reactants. The amount of heat released for each type of chemical reactions can be calculated by applying the principle of stoichiometry; this is done through the use of species transport and finite volume chemistry model in FLUENT. In truth, the enthalpy of formation varies with surrounding temperature, which in turns directly affects the amount of heat released from combustion. This effect of temperature variation has been studied in Huang's work [5] and according to his findings; the effect has been proven to have little quantitative effect on heat energy release. This study has neglected the variation of heat energy release due to the effect of temperature change in the surroundings; instead it has been based on the enthalpy values on a reference temperature of 281.3 Kelvin.

B. Particle-Gas Dynamics

As gas interact with the falling particles, it collides with some of the particle while passes through others. The passage which the gas passes through is called voidage, as the energized gas travels upwards through this voidage, it losses energy and hence losses pressure. Other particles interacts with the upward travelling gas receive the impulse and gain momentum, the resulting force causes motion from each particle which in turn interacts with the neighbor particles. As a result of particle-fluid interaction force, the gravitational force and the inter-particle forces between each particle obtain the translational and angular velocities.

C. Heat Transfer

Heat transfer in the packed bed system of shaft kiln can be considered to consist of the following modes:

1) Conduction heat transfer in axial and radial direction between the particles in the bed.
2) Convective heat transfer between the bed particles and the flowing gas.
3) Heat transfer due to the effect of the convective mode on the conduction.
4) Heat transfer due to the radiation.
    a. between the bed particles
    b. between the flowing gas and bed wall
    c. between the particle and the flowing gas
5) Heat transfer from wall to bed particles.
    a. bed wall and bed particles
    b. bed wall and the flowing medium

III. PROCESS SIMPLIFICATION

The process that takes place inside a shaft kiln is complex. In order to describe the process quantitatively and to yield a more robust solution some simplification were made as summarized below:

1) The process inside the kiln is asymmetrical. Hence, it is believed that a 2D model should be adequate to capture heat profiles and physical characteristics of the particle-gas interaction inside the kiln.
2) The combustion inside the shaft kiln is assumed to be complete combustion. This assumption is made from the fact that the amount of primary air and secondary air, which contributes in the combustion process, is much higher than that of Natural gas.
3) The insulation system of shaft kiln at reference plant is known to be at least 93.5% efficient. Therefore, heat transfer through wall can be considered insignificant.
4) Only CH_4 and O_2 combustion is considered. It was assumed that the properties of combustible components in natural gas are identical to those of methane. With the exclusion of methane, other gas species made up of approximately 12.12%. The percentage of natural gas contribution to the process gas during normal operation is only 8.36%; therefore, the overall composition of other gas component except methane is 1.04%. This has been considered to be negligible.

5) Equivalent spherical diameter was used instead of specifying real dimension of the MgO briquettes (prolate spheroid).

IV. NUMERICAL APPROACH

Numerical computation of fluid transport includes conservation of mass, momentum and energy, chemical species concentration and turbulence models. GAMBIT was used as a preprocessor to create the geometry, discretize the fluid domain into small cells to form a volume mesh or grid and set up the appropriate boundary conditions. The flow properties were then specified and the problems were solved and analyzed by FLUENT solver.

The basis of modeling of an incompressible Newtonian fluid flow module is the use of the conservation of mass equations, given by

$$\frac{\partial \rho}{\partial t} + \vec{\nabla} \cdot (\rho \vec{V}) = 0 \quad (1)$$

And the Navier-Stokes equation in x, y and z direction given by,

$$\frac{\partial(\rho u)}{\partial t} + \vec{V} \cdot \vec{\nabla}(\rho u) = -\frac{\partial p}{\partial x} + \vec{\nabla} \cdot (\mu \vec{\nabla} u) + \rho g_x \quad (2)$$

$$\frac{\partial(\rho v)}{\partial t} + \vec{V} \cdot \vec{\nabla}(\rho v) = -\frac{\partial p}{\partial y} + \vec{\nabla} \cdot (\mu \vec{\nabla} v) + \rho g_y \quad (3)$$

$$\frac{\partial(\rho w)}{\partial t} + \vec{V} \cdot \vec{\nabla}(\rho w) = -\frac{\partial p}{\partial z} + \vec{\nabla} \cdot (\mu \vec{\nabla} w) + \rho g_z \quad (4)$$

The governing equations can be generally written as follows for a given property (in this case arbitrarily property is assigned by the symbol ϕ):

$$\frac{\partial(\rho\phi)}{\partial t} + div(\rho\phi u) = div(\Gamma\, grad\ \phi) + S_\phi \quad (5)$$

where first and second term of the left hand side represent the rate of increase of ϕ in fluid element (transient) and net rate of flow of ϕ in the fluid element (convective) respectively. At the right hand side, the first term represents the rate of increase of ϕ due to diffusion and second term is the rate of increase of ϕ due to sources. This equation is integrated with respect to a control volume of fluid, as given by (for a steady state non time dependant flow),

$$\int_{CV} \frac{\partial(\rho\phi)}{\partial t} dV + \int_{CV} div(\rho\phi u) dV = \int_{CV} div(\Gamma\, grad\ \phi) dV + \int_{CV} S_\phi dv V \quad (6)$$

The turbulence model used in this model was the Standard k - ε model. Here k is the turbulent kinetic energy and ε is the rate of viscous dissipation. The transport equations for k and ε can be given by,

$$\frac{\partial(\rho k)}{\partial t} + \frac{\partial}{\partial x_j}(\rho u_j k) = \rho P - \rho\varepsilon + \frac{\partial}{\partial x_j}\left[\left(\mu + \frac{\mu_t}{\sigma_k}\right)\frac{\partial k}{\partial x_j}\right] \quad (7)$$

$$\frac{\partial(\rho\varepsilon)}{\partial t} + \frac{\partial}{\partial x_j}(\rho u_j \varepsilon) = C_{\varepsilon_1}\frac{\rho P \varepsilon}{k} - C_{\varepsilon_2}\frac{\rho\varepsilon^2}{k} + \frac{\partial}{\partial x}\left[\left(\mu + \frac{u_t}{\sigma_\varepsilon}\right)\frac{\partial \varepsilon}{\partial x}\right] \quad (8)$$

To accurately represent the turbulent flow, turbulence intensity and length scale must be specified for each of the velocity boundary surface. Turbulence intensity defines the ratio of the root-mean-square of the velocity fluctuation to the mean flow velocity. Length scale is a physical quantity relates the size of the large eddies that contain in the energy in turbulent flows. They can be identified from the following equations,

$$I = 0.16\,(\mathrm{Re})^{-1/8} \quad (9)$$

$$\mathrm{Re} = \frac{vD}{\nu} \quad (10)$$

$$l = 0.4 \times T_{BL} \quad \text{For wall bound flow} \quad (11)$$

$$D_H = L \quad (12)$$

Turbulence intensity and length scale can be applied to velocity boundary condition for secondary air inlet while, hydraulic diameter must be used for gas and primary air inlet. The above equations were integrated, representation being implemented and applied to the discretised flow geometry. The finite volume method was used to descretize the partial differential equations of the model. A number of methods were used to ensure that the solver converges to a solution and that the solution is reasonable. These include a check with Bernoulli's equation and the solver.

V. COMPUTATIONAL METHODOLOGY

A CFD solver, FLUENT6.2 was employed to reproduce the conditions described in previous sections. To obtain a prediction, three main components of CFD codes must be completed this include mesh generation, solving the problem and post processing. The geometry of the vertical shaft kiln used in this work was in 1:1 scale to the real kiln and was constructed using GAMBIT as shown in Fig.3. The labels displayed are the boundary conditions specified to each surface.

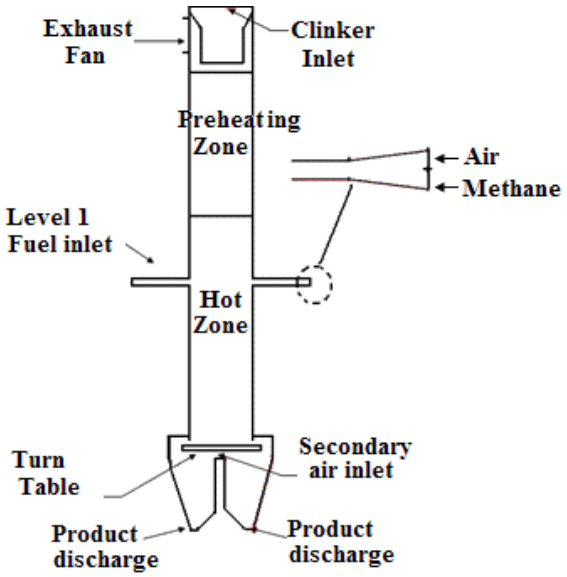

Fig.3 Geometry of vertical shaft kiln

The geometry of the kiln consists of two main zones, one around the burner level (hot zone) and another above it (Preheating zone). Note that only level one fuel inlet injector is included in the geometry. Author deliberately left the other 3 levels out when the geometry was constructed, as during the time the model was being developed the first burner level are being used at the referenced plant. Moreover, it has been known that build up of scale above the burner level is part of

the characteristics of the shaft kiln. It is believed that the buildup is mainly caused by the vigorous heat transfer and high gas velocities occur in the region just above the burner level, causing the stagnant condition of particle flow and molecular bonding of MgO in that region. Although formation of scaling is not included in the scope, however, author planned to use this as one of the few conditions for model validation. For this reason, the modeling of the other three burner levels was not included.

Quadrilateral mapped grid and paved grid were used to construct the unstructured mesh. Quadrilateral cell was chosen, as suggested by FLUENT 6.2 user guide, to be the suitable grid topology for multiphase flow problem [6]. In constructing the grid, one major issue encountered was the creation of the turning plate, where a face must be subtracted from another to create a solid zone inside a fluid zone. Finally, a variety of mesh spacing were constructed and tested, however by using solution stability, accuracy and computational time as the main criteria for selection, 5 cm mesh spacing was selected as the optimal size, except for 1 cm mesh spacing selected for the fuel inlet. Moreover, boundary layers were specified to all wall surfaces to ensure more accurate reproduction of turbulence flow of gas in fuel inlet pipes and in the shaft kiln.

The computational model consisted of two sub-models, species transport and finite volume chemistry for combustion, and multiphase Eulerian finite volume model for particle dynamics and heat transfer of gas and packed bed. The methodology utilized to solve and couple each model is summarized below:

1) A steady state segregated solver was used to solve energy and momentum conservation equations from species transport and finite volume chemistry, multiphase Eulerain finite volume models.
2) The discretization of density and pressure interpolation was achieved by applying first order upwind scheme.
3) The phase couple simple algorithm method was employed for pressure and velocity coupling.
4) Porous media was specified to the regions where the reproductions of packed bed of MgO briquettes are required.

VI. Simulation conditions

Due to program limitation, continuous moving packed was reproduced defining the packed bed as "stationary porous fluid zone" with granular fluid phase flowing through it. By specifying the solid particle as granular fluid, it could be assumed that it behaves like a bulk of fluid. To initiate the simulation, first, the control variables such as primary air inlet velocity, secondary air inlet velocity, methane inlet velocity, exhaust pressure, product input, output and turning plate rotational speed were specified to their corresponding inlet or outlet boundary. Once the simulation was initiated the simulation continues until no obvious change was observed in the residual plot of energy and momentum transfer in both phases, under which condition, the simulation was regarded as steady state. Initial conditions, boundary conditions and physical properties of material used in the model are summarized in Tables 1, 2 and 3 respectively. A non zero mass fraction was specified to CH_4 to ignite the combustion in fewer iterations.

Table 1. Initial conditions used in simulation

Description	Values
Volume fraction of Hot Zone	0.577
Volume Fraction of Preheat Zone	0.167
Temperature of Hot Zone	1300 C
Temperature of Top Kiln Zone	300 C
Gas Temperature	300 C
Air temperature	300 C
CH_4 Mass Fraction	0.2
O_2 Mass Fraction	0.23

Table 2. Boundary conditions used in simulation

Description	Type	User Input
Shaft kiln and chute walls	Stationary Wall	-
Fuel injector pipe	Stationary Wall	-
Primary Air Inlet	Velocity Inlet	30 m/s
Secondary Air Inlet	Velocity Inlet	34 m/s
Gas Inlet	Velocity Inlet	5.84 m/s
Exhaust	Exhaust Fan	101 kPa
Turning Plate	Rotating Wall	1.5 rad/s
Hot Zone	Porous Zone	0.467
Top Zone	Porous Zone	0.467
Product outlet	Velocity Inlet	0.0232
Raw material Inlet	Velocity Inlet	0.00032 m/s
Mass content of O_2	Velocity Inlet	0.23
Mass content of CH_4	Velocity inlet	1

Table 3. MgO physical properties used in simulation

Physical Properties	Value
Bulk density of deadburned MgO	3410 Kg/m^3
Bulk density of raw MgO	1910 Kg/m^3
Theoretical Bulk density of MgO	3580 Kg/m^3
Specific gravity	40.304 g/mol
Enthalpy of formation of MgO	-0.601 J/mol
Porosity of deadburned MgO	0.047
Porosity of raw MgO	0.467
Volume fraction of raw MgO	0.167
Volume fraction of deadburned MgO	0.523
Equivalent Diameter of raw MgO	0.06214 m
Equivalent Diameter of deadburned MgO	0.03 m
Angle of internal Friction	30
Granular viscosity	Gidspaw
Granular Bulk viscosity	Lun-et-al
Frictional viscosity	Schaeffer

Granular temperature	Algebraic
Solid Pressure	Lun-et-al
Radial Distribution	Lun-et-al
Elasticity Modulus	derived
Packing limit	0.5

Since the specific heat capacity (Cp) and thermal conductivity of MgO briquettes are both dependent on temperature, a set of values were entered in FLUENT using piecewise linear function to determine the values at corresponding temperatures. Values of specific heat and thermal conductivity of MgO briquettes for a range of temperatures were acquired from [7] and [8]. Specific heat capacity for temperature of 300K-1200K only were given in [7], however by using Microsoft Excel the specific heat capacity of MgO briquettes at temperature higher than 1200 K were determined using the Logarithmic trend line as shown in Fig.4. Table 4 shows the value of thermal conductivity of MgO briquettes used in simulation.

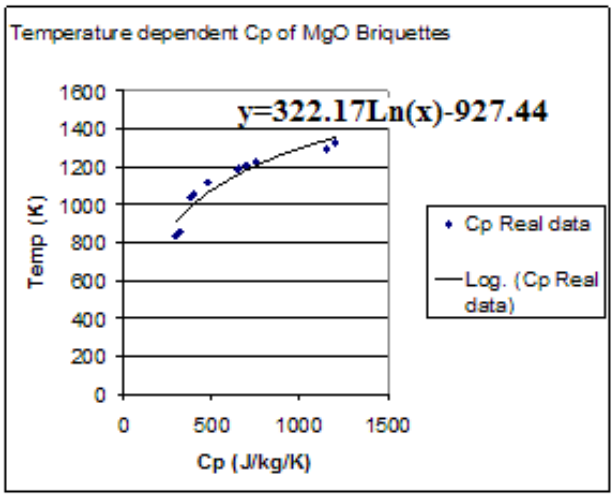

Fig.4 Cp of MgO (data point acquired from [7])

Table 4. Thermal conductivity of MgO [8]

Temperature (K)	Thermal Conductivity (W/kg/K)
273	42
373	33.494
673	5.861
1073	5.024
1473	4.604
1873	4.815
2273	5.443

VII. Result and Discussion

Only data available for model validation is shown in Fig.5. This is design temperature data as a function of height of the kiln for the reference plant. It should be noted, however, that the diameter and cooling system at existing kiln is slightly different from the originally designed one due to recent modification. The diameter of the existing kiln (Fig.1) is about 10% larger than the one shown in Fig.5 (originally installed kiln) and the cooling air (i.e. secondary air) enters the existing kiln from the bottom whereas it enters the originally designed kiln from the sides.

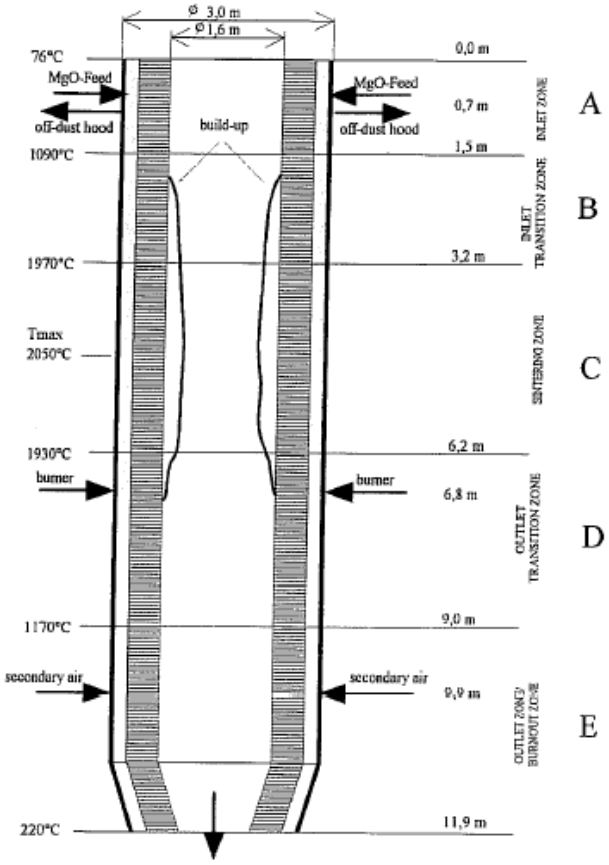

Fig.5 Schematic diagram of design temperature of the original kiln as a function of height

Fig.6 shows the simulated contour of gas temperature at steady state. The preheating zone is at the top of the kiln where heat lost to new feed of MgO causes the decrease in gas temperature. The cooling is at the bottom of the kiln where secondary air is preheated by downwards moving hot deadburned products. The burning zone is around the fuel distributor level where most of the sintering process takes place. It is also obvious that the heat profiles close to the walls and around the burner level are distinctively higher than in other regions, this indicates the formation of MgO scaling which is caused by molecular bonding at high temperatures. It can be seen from Fig.6 that the maximum temperature of methane without heat transfer to other material is around 2250 to 2350 K. This gives the percentage error of 3%-7% when compared with the theoretical maximum burning temperature of methane, which is 2421K [9].

The gas temperature profiles obtained from simulation are compared with the design data in Figs.7a, 7b and 7c. It can be seen from Fig.7 that the simulated profiles displays similar trends as that of the design data. The unexpected differences in temperature at point A in Fig.7 for the left and right walls could be due to the difference in cooling system of the existing kiln as mentioned earlier. In Fig.7c, a much higher

temperature of gas is shown below the burner level in existing kiln than that of the original kiln this indicates inefficiency in the cooling system of the existing kiln.

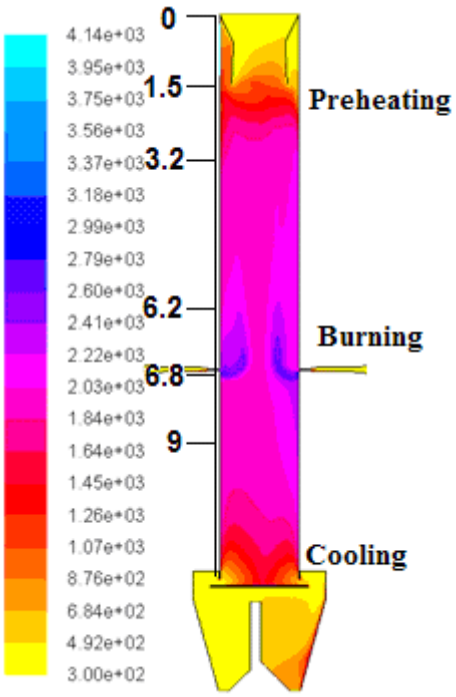

Fig.6 Contour of gas temperature at steady state

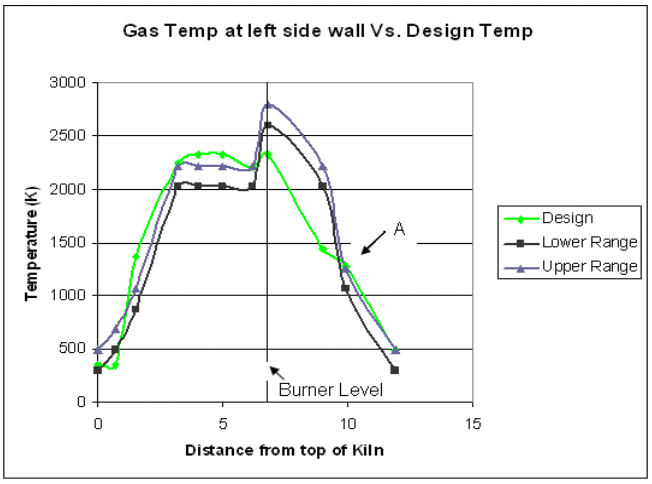

Fig.7a Gas heat profile (left wall) vs design profiles

It should be noted that in region between the burners to the height of 9.9 m from the top of the kiln, the temperature obtained from the simulation is much higher than that of the design values. The factor contributing to this is the difference of cooling system. The existing kiln at reference plant has the secondary air enters the kiln from the bottom of the turn table, whereas the cooling air enter the design kiln from the side as shown in Fig.5. From Fig.5 the cold air injector are located at 9.9 meter from top of the kiln which corresponds to point A in Figs. 7a and 7b. Since the location of secondary air inlet is higher in the design kiln, it means that air temperature entering the kiln at 9.9 m would be lower than that of the existing system, where the air is preheated before reaches the 9.9 m level. Therefore, when the cooler air moves upwards, the temperature at each reference point would be lower. However, the cold air in the old kiln would have received similar amount of heat from the downwards moving deadburned, causing the air temperature below the 9.9 meter reference point to be similar to that obtained from the simulation. Moreover, it can also be seen that the temperature above the burner level near the wall region is much higher than the rest; this gives a good indication of development of MgO scales on the walls due to high temperature which causes the molecular bonding of MgO briquettes to the refractory wall which also made of MgO bricks.

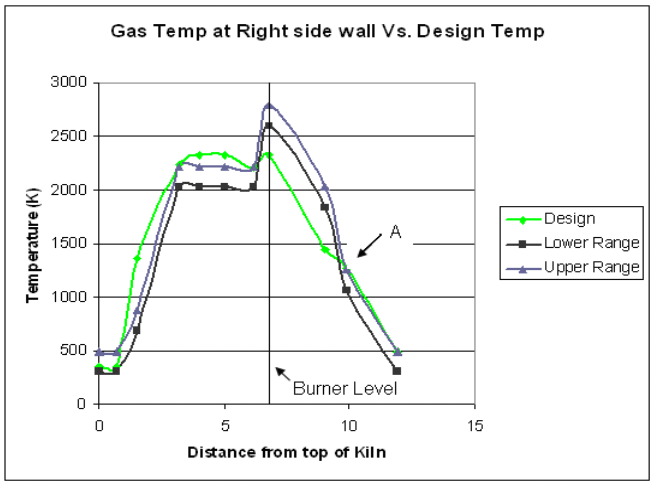

Fig.7b Gas heat profile (right wall) vs design profiles

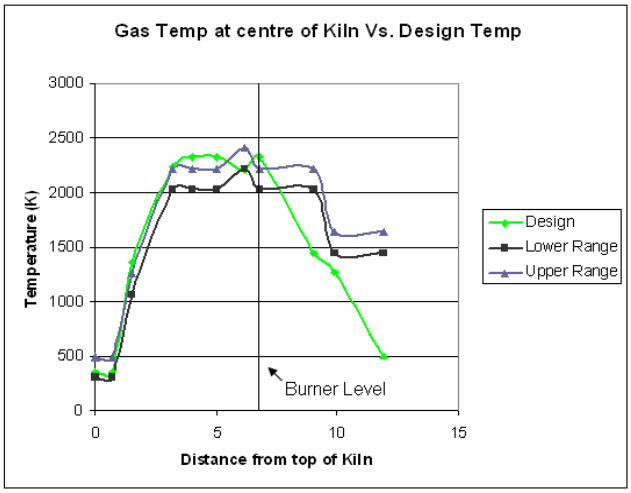

Fig.7c Gas heat profile (Centre) vs design profiles

Fig. 8 compares granular solid phase temperature profile with gas temperature along the left side wall, right side wall and center of the kiln. It can be seen from Fig.8 that the granular phase temperature profile follows that of gas temperature profile in the higher regions of the kiln. However, the granular and gas temperatures on each side of the kiln and at the centre are different. This is a result of both the physical interaction of porous media and gas, and the exhaust system

which positioned on the top left hand corner of the kiln; influencing the air and gas flows to swirl towards one side more than another. Moreover, constant temperature profiles of granular phase below the burning level indicate inefficiency in the existing cooling system. Despite these differences, it can be seen that as the secondary air enters the existing kiln it moves upwards absorbing temperature from the hot dead burned briquettes and eventually enter the burning zone where the temperature of gas peaks at around 2200 K to 2500 K. The gas temperature progressively reduced as it moves upwards giving off heat to the briquettes and eventually reduced to around 350 K to 500 K prior to exhaust.

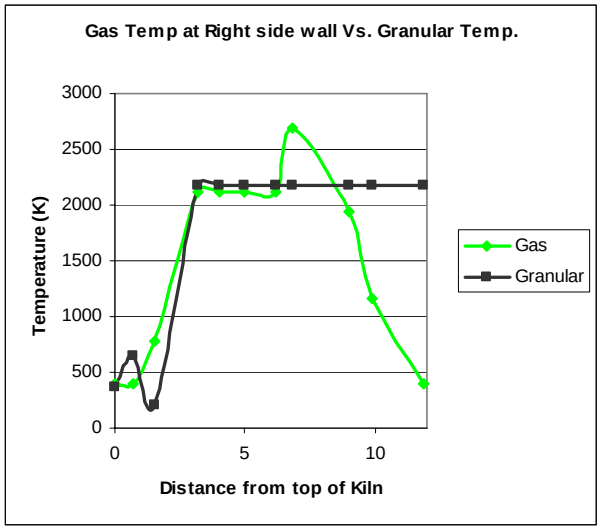

Fig.8a Left side wall gas temperature vs granular temperature

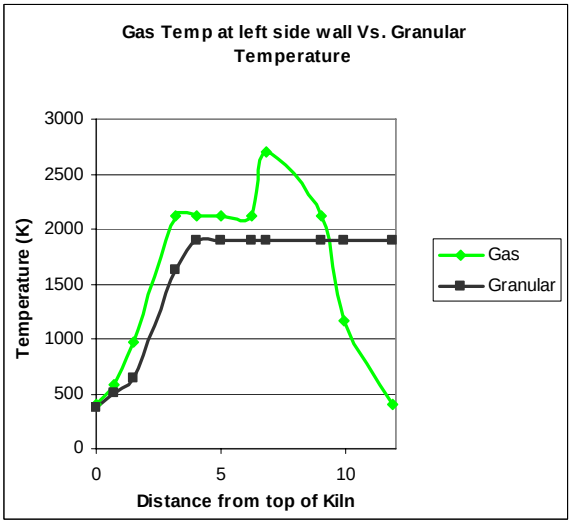

Fig.8b Right side wall gas temperature vs granular temperature

Although, the gas temperature profiles shows reasonable agreement with the design profiles (Fig.7) but the results obtained from the analysis of particle dynamics suggest that there is a discrepancy in the model (Fig.8). Assumption made earlier that the "solid particles" behaves like a "granular fluid (i.e. bulk of fluid)", may not be appropriate and thus prevents the model from reproducing the correct physics of solid grain structures. It was observed during the simulation that, as simulation progressed towards the steady state the packed bed began to expand and float towards the exhaust. This was due to the packed bed behaving like a fluidized bed. Because an amount of particles still move downwards and there is still continuous feed of new materials into the kiln, the effect of this discrepancy could not be detected in the gas temperature profile. Due to this fact, further study is recommended on gas-particle dynamics in order to establish correct modeling of shaft kiln thermodynamic processes.

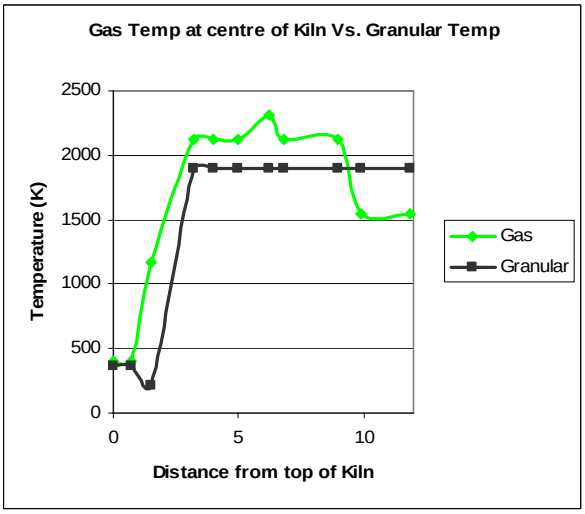

Fig.8c Centre of kiln gas temperature vs granular temperature

VIII. Conclusions and Recommendations

A 2D CFD model has been developed to simulate thermodynamic processes of shaft kiln of sintering magnesia briquettes. The model showed reasonable agreement with the design values of gas temperature profile, however, discrepancy in the model was observed for gas-particle dynamics. Further work is needed for a more accurate prediction of gas and particle dynamics interactions. It is highly recommended that a 3D CFD model should be developed using user-defined functions which can be written in C++ language and embedded in FLUENT.

Appendix

Nomenclature

$C_{\varepsilon 1}$, $C_{\varepsilon 2}$	Constants
D	Diameter of region where fluid is entering (m)
D_H	Hydraulic diameter (m)
g	Gravity (m/ s^2)
I	Intensity
k	Turbulent kinetic energy (m^2/s^2)
L	Diameter of the pipe of the shaft kiln (m)
l	Length scale (m)
Re	Reynolds number
u,v,w	Velocity component in x, y and z direction (m/s)
$\vec{\nabla}$	Velocity field

v Mean velocity of fluid in equation 10
S_Φ User-defined source terms
S Modulus of the mean rate of strain tensor
T_{BL} Thickness of boundary layer (m)

Greek symbols

ε Turbulent dissipation rate (m^2/s^3)
μ Dynamic viscosity (N.s/ m^2)
ν Kinematic viscosity (m^2/s)
ρ Density (kg/m^3)

REFERENCES

[1] D. Saotayanan, "CFD Modeling of Vertical Shaft Kiln," Bachelor of Engineering Thesis, Faculty of Sciences, Engineering and Health, Central Queensland University, Rockhampton, Australia, 2007.
[2] Project Profile, Reference Plant (Operations) Pty Ltd, 1993.
[3] M. Erskine, "Lotus-123 Spreadsheet Based Shaft Kiln Model," Reference Plant Internal Report, 1996.
[4] B. (Michael) Huang, "Computer Model of the shaft Kiln Process," Master of Engineering Thesis, Department of Electrical Engineering, Central Queensland University, Australia, 1999.
[5] B. Huang, K. Kwong and M. McQuade, "Mathematical Modeling of a Vertical Shaft Kiln," in *Proc. National Heat Transfer Conference*, Albuquerque, New Mexico, USA, 15-17 August, 1999.
[6] FLUENT 6.2, User Manual, FLUENT Inc.
[7] Physics and Chemistry, Journal of Research of the National Bureau of standards-A. Vol G7A, No 4, July – August, 1963.
[8] An Investigation into the Wear Phenomenon of Magnesia Refractory Bricks in the Vertical Shaft Kilns (1995), Carsten Schwiderek, Department of Chemical Engineering, University of Dortmund, Germany.
[9] http://en.wikipedia.org/wiki/Methane/, viewed 6/5/07.

Mohammad G. Rasul graduated in Mechanical Engineering from Bangladesh University of Engineering and Technology (BUET), Dhaka, Bangladesh in 1987. He completed his Master of Engineering in Energy Technology from Asian Institute of Technology (AIT), Bangkok, Thailand, in 1990. He obtained PhD on Energy and Thermodynamics from The University of Queensland, Australia, in 1996.

Currently, he is working as a Senior Lecturer in Mechanical Engineering at College of Engineering and the Built Environment, Faculty of Sciences, Engineering and Health, Central Queensland University, Rockhampton, Queensland 4702, Australia. He is specialised and experienced, and interested in research, teaching and consultancy in the area of thermodynamics and energy, fluid mechanics, process industry's energy and environmental pollution analysis and building energy analysis.

Dr Rasul is an author of more than 80 refereed journal and conference papers including few chapters in books. He is an active member of the Engineers Australia and the Australasian Association for Engineering Education (AAEE).

D. Saotayanan graduated in Mechanical Engineering from Central Queensland University in 2007. His research interest includes thermofluid engineering and mining technology. Currently, he is working as a Graduate Mechanical Project Engineer at Xstrata Zinc, Lead Smelter, Mount Isa, Australia.